2.6 HOW MUCH RAIN REACHES THE SURFACE?
LESSONS LEARNED FROM VERY HIGH RESOLUTION OBSERVATIONS
IN THE GOODWIN CREEK WATERSHED

Matthias Steiner* and James A. Smith
Princeton University, Princeton, NJ

Lisa C. Sieck and Stephen J. Burges
University of Washington, Seattle, WA

Carlos V. Alonso
USDA/ARS National Sedimentation Laboratory, Oxford, MS

1. INTRODUCTION

Rainfall is highly variable in space and time, depending on the synoptic, mesoscale and storm-scale forcing. This variability affects our capability to measure rainfall from in-situ as well as remote-sensing perspectives. The lack of continuous observations in space and time requires a merging of information obtained from various sources. The variability of rainfall within the range of sensor resolution differences, however, has a significant effect on the comparison between observations made by instruments with differing resolutions in space and time. For example, a radar and rain gauge may both measure rainfall perfectly and accurately, from an instrument and retrieval perspective, yet they do not record the same phenomena (e.g., Austin 1987; Kitchen and Blackall 1992; Ciach and Krajewski 1999). The rainfall amounts estimated by both types of instruments are likely burdened by measurement limitations and uncertainties. One key question is how much of the observed variance between radar and gauge observations can be explained simply by sensor resolution differences, combined with the space-time variability of rainfall?

Detailed observations of rainfall at very high resolution in space and time have been carried out for the 21 km^2 Goodwin Creek research watershed (Fig. 1) in northern Mississippi (Steiner et al. 1999; Alonso and Bingner 2000). The comprehensive setup of instrumentation includes more than 30 rain gauges, two Joss-Waldvogel (1967) raindrop disdrometers, and observations of the low-level wind profile at the climate station (Fig. 2) in the center of the catchment (latitude 34° 15' 16" N, longitude 89° 52' 26" W). This site also hosts a SURFRAD network station (Hicks et al. 1996).

The Goodwin Creek research watershed is under coverage from four WSR-88D radars (Heiss et al. 1990), the closest located in Memphis, Tennessee. Moreover, very high resolution radar observations (50 m by 1 deg in space, tens of seconds in time) have been made using the mobile Doppler-on-Wheels (DOW) radar (Wurman et al. 1997) for a selection of storms passing over the Goodwin Creek area (Fig. 3).

The data are used to evaluate measurement issues ranging from the rain gauge catch to the radar rainfall estimation. Analyses of the rainfall variability observed at very small space and time scales will show how this variability affects the radar-gauge comparison. The results will provide guidance for effectively merging information from various sources to yield the best surface rainfall estimates.

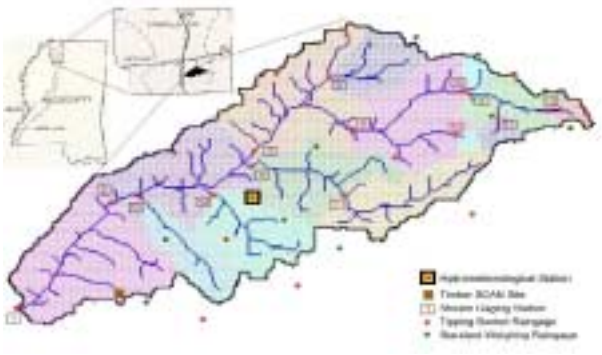

Figure 1. Geographical location and outline of the Goodwin Creek research watershed in northern Mississippi.

* *Corresponding author address*: Dr. Matthias Steiner, Department of Civil and Environmental Engineering, Princeton University, Princeton, New Jersey 08544; phone: 609/258-4614; email: msteiner@princeton.edu

Figure 2. Station 50 in the center of the Goodwin Creek watershed hosting a variety of above-ground and buried rain gauges, raindrop disdrometers, wind profile measurements, and the SURFRAD station.

Figure 3. Doppler-on-Wheels (DOW) radar owned by the University of Oklahoma.

2. STORM OF 23-24 APRIL 2001

Data collected during a major storm system that passed over the Goodwin Creek watershed in northern Mississippi on 23-24 April 2001 (Fig. 4) are used to demonstrate a range of uncertainty involved in the in-situ measurement and remote sensing of rainfall. These uncertainties are related to both measurement caveats and differences in sampling volumes.

Figure 5 shows the storm at the time of most intense rainfall over the catchment, as seen by the Memphis WSR-88D (KNQA) radar, operating at 10 cm wavelength. The center of the Goodwin Creek watershed is approximately 120 km due south of the KNQA radar. The precipitation appeared to be organized into an intense line of convection as it passed over the catchment. However, a closer look taken with the (3 cm) DOW radar, deployed at the upper end of the Goodwin Creek watershed, reveals significant small scale structures within that convective line (Fig. 6). These details seen by the DOW radar at 50 m resolution cannot be resolved by the WSR-88D, which has only a 1-2 km resolution at that range. The vertical cross sections collected by the DOW (Fig. 7) illustrate with great detail how air is lifted along the frontal boundary and precipitation formed. However, Fig. 7 also shows the potentially severe limitations of shorter-wavelength radar measurements suffering from signal attenuation in heavy rainfall. This attenuation is demonstrated by the complete loss of signal in radial direction behind that intense cell of convection.

Figure 4. IR cloud top brightness temperatures as seen by the GOES-8 satellite on 24 April 2001 at 0015 UTC.

Figure 8 shows the storm passage over the center of the Goodwin Creek watershed from a surface meteorological perspective. A significant drop in temperature (Fig. 8a) and a wind shift from approximately southerly to northwesterly direction (Fig. 8b) occurred with the frontal passage. The winds ahead of the front fluctuated around 5 m/s, but calmed to less than 2 m/s after the frontal passage. Surface rainfall came in several bursts with maximum rain rates reaching 140 mm/h (at 2319 UTC), accumulating close to 30 mm of rain (Fig. 8c).

The raindrop size distributions observed by the disdrometer in the center of the catchment show significant storm variability, which results in

uncertainty of the relationship between radar reflectivity and rain rate (Fig. 9). Overall, the relation $Z=300R^{1.4}$ provides a good fit through the data. This relationship was thus used to convert radar reflectivity to rainfall rate when deriving the KNQA radar-based rainfall accumulation for the storm (Fig. 10). The largest storm total rainfall amounts (> 50 mm) were observed more than 20 km to the southeast of the catchment (Fig. 10a). The radar-estimated rainfall depth varied across the Goodwin Creek watershed (Fig. 10b), with mean, minimum, and maximum accumulation of 25.5 mm, 12.3 mm, and 36.0 mm, respectively.

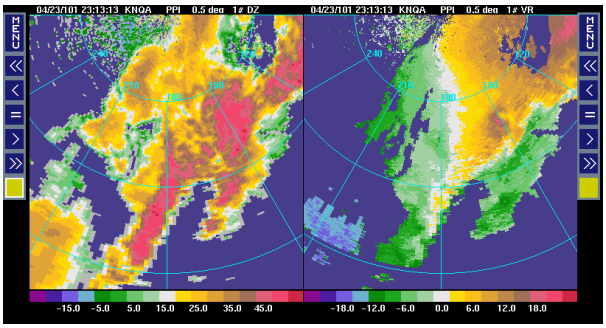

Figure 5. Radar reflectivity (left panel) and radial Doppler velocity (right panel) observed by the Memphis WSR-88D (KNQA) radar on 23 April 2001 at 2313 UTC. The resolution is 1 km in radial direction and 1 deg in azimuth. Range rings are shown at 50 km intervals.

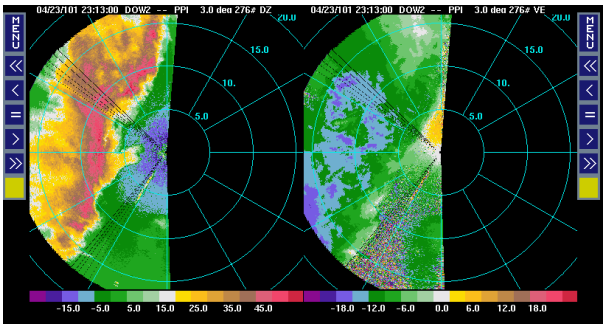

Figure 6. Radar reflectivity (left panel) and radial Doppler velocity (right panel) observed by the Doppler-on-Wheels (DOW) radar on 23 April 2001 at 2313 UTC. The resolution is 50 m in radial direction and 1 deg in azimuth. Range rings are shown at 5 km intervals.

The Goodwin Creek rain gauge network consists of several different types of instruments, namely, Belfort weighing gauges (BEL), Texas Instruments tipping bucket gauges (TXI), USDA Agricultural Research Service tipping bucket gauges (ARS), one Australian Hydrologic Service tipping bucket gauge (TB3), and simple buried collectors (COL). In addition, two Joss-Waldvogel raindrop disdrometers (DIS) are located at the climate station (station 50). This central site hosts at least one gauge of each type deployed across the catchment. One tipping bucket gauge is mounted above ground (sARS), while another is buried in the ground (bARS).

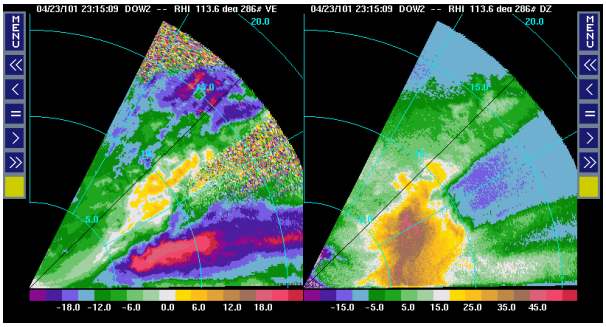

Figure 7. Vertical cross section (towards west in Fig. 6) of radar reflectivity (left panel) and radial Doppler velocity (right panel) observed by the Doppler-on-Wheels (DOW) radar on 23 April 2001 at 2315 UTC. The resolution is 50 m in radial direction and 1 deg in azimuth. Range rings are shown at 5 km intervals.

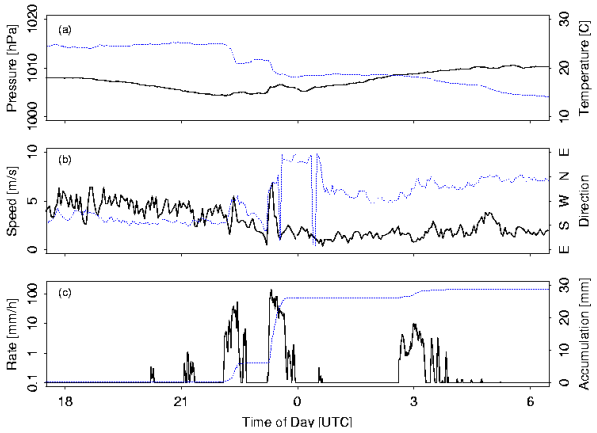

Figure 8. Time series of pressure, temperature (top panel), wind speed and direction (middle panel), and rainfall intensity and rain accumulation (bottom panel) as observed at the climate station in the center of the catchment on 23-24 April 2001.

The collected water in the BEL gauges is measured after the storm to compare with the amount recorded on the chart. Moreover, we have

developed water collection devices for some of the ARS and TXI tipping bucket gauges and the TB3, providing an independent measure of rainfall for these gauges. Detailed calibration curves have been established for most gauges to correct for rain rate dependent effects. COLs were buried next to several of the gauges to obtain a best estimate of the rainfall reaching the surface not affected by wind.

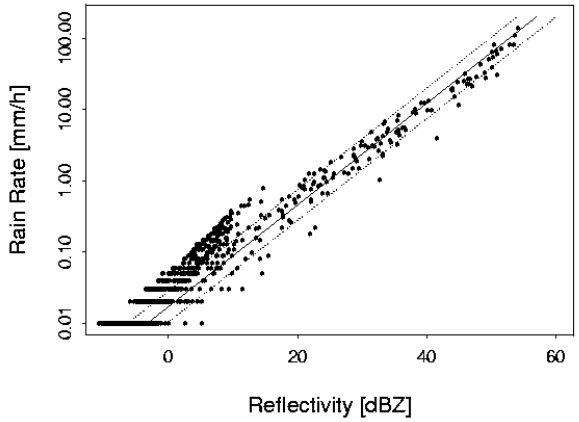

Figure 9. Variability of raindrop size distributions and effect on the reflectivity-rain rate relationship for the storm of 23-24 April 2001. Solid line shows a Z-R relationship with multiplicative factor A=300 and power factor b=1.4, while dotted lines show relationships with A=600 and A=150, respectively.

Table 1 shows a compilation of the rainfall information obtained for the 23-24 April 2001 storm passing over the Goodwin Creek watershed. The instruments worked properly, with the exception of a few rain gauges (5, 6, and 62) that were malfunctioning and one disdrometer (DIS2) that was down. Although the calibration for two of the Belfort weighing rain gauges (50 and 57) was somewhat questionable, this gauge type was the most reliable. This is due to its sturdy design and built-in capability for redundant measurements (i.e., chart recording of weighed rain amount, plus collection of total water). The tipping bucket rain gauges are more prone to malfunctioning. In addition, the calibration of the ARS gauges varied by ±10%. The TXI gauges was more stable, but their calibration also varied by up to +10%. The wind effect on the rain gauge catch, estimated by comparing the above-ground to the buried rainfall amounts, was on the order of a few percent (1%-4%). The collection of the water flowing through the ARS and TXI gauges was difficult, however, the agreement with the tip-based amounts was encouraging. The radar-gauge comparison is clearly affected by sensor resolution differences and the storm rainfall variability, as demonstrated by Fig. 10b and Table 1.

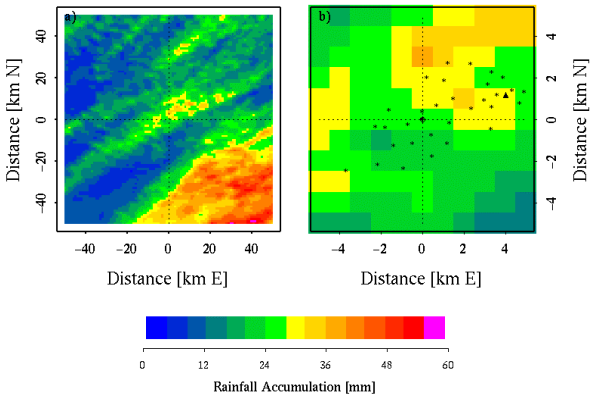

Figure 10. Rainfall accumulation estimated based on the Memphis WSR-88D radar for the storm of 23-24 April 2001 and a domain with side length of 100 km **(a)** and 10 km **(b)**, respectively, centered on the Goodwin Creek watershed. The rain gauge locations (∗), the climate station (■), and the DOW radar site (▲) are shown as well.

3. CONCLUSIONS

Detailed observations of a major storm system that passed over the small, but well instrumented Goodwin Creek research watershed in northern Mississippi were used to highlight the range of uncertainty encountered measuring rainfall from an in-situ to remote sensing perspective. These uncertainties are related to the:

1) *rain gauge measurements*
   - calibration curve for tips is dependent on rain rate, and may vary from gauge to gauge
   - wind effect is a function of gauge design, wind speed, and raindrop size, and tends to reduce the gauge catch
2) *radar rain measurements*
   - sampling volume and height of center of beam above the ground increase with increasing distance from radar site
   - potential contamination of radar echo by ground clutter, bright band (i.e., melting layer signature), and graupel or hail
   - variability of raindrop size distributions and thus uncertainty in the relationship between radar reflectivity and rain rate
   - inhomogeneous beam filling or overshooting of cloud tops at far ranges

3) merging of information

- sampling volume and sensitivity differences
- mismatches in space and time

These factors burden individual measurements and affect the comparison and merging of information used to obtain the most reliable rainfall estimates. This study aims to quantify these sources of uncertainty and ultimately provide guidance for designing appropriate rainfall measurement networks.

Acknowledgments. This project is supported by NSF Grant EAR-9909696. The extraordinary assistance provided by the staff of the National Sedimentation Laboratory in Oxford, and Donald Giuliano and Steve McDonald of the University of Oklahoma is greatly appreciated.

REFERENCES

Alonso, C. V., and R. L. Bingner, 2000: Goodwin Creek Experimental Watershed: A unique field laboratory. *ASCE, J. Hydraulic Eng*., **126**, 174-177.

Austin, P. M., 1987: Relation between measured radar reflectivity and surface rainfall. *Mon. Wea. Rev*., **115**, 1053-1070.

Ciach, G. J., and W. F. Krajewski, 1999: On the estimation of radar rainfall error variance. *Adv. Water Resour*., **22**, 585-595.

Heiss, W. H., D. L. McGrew, and D. Sirmans, 1990: NEXRAD: Next Generation Weather Radar (WSR-88D). *Microwave J*., **33**, 79-98.

Hicks, B. B., J. J. DeLuisi, and D. R. Matt, 1996: The NOAA Integral Surface Irradiance Study (ISIS)—A new surface radiation monitoring program. *Bull. Amer. Meteor. Soc*., **77**, 2857-2864.

Joss, J., and A. Waldvogel, 1967: Ein Spektrograph für Niederschlagstropfen mit automatischer Auswertung. *Pure Appl. Geophys*., **68**, 240-246.

Kitchen, M., and R. M. Blackall, 1992: Representativeness errors in comparisons between radar and gauge measurements of rainfall. *J. Hydrol*., **134**, 13-33.

Steiner, M., J. A. Smith, S. J. Burges, C. V. Alonso, and R. W. Darden, 1999: Effect of bias adjustment and rain gauge data quality control on radar rainfall estimation. *Water Resour. Res.*, **35**, 2487-2503.

Wurman, J., J. Straka, E. Rasmussen, M. Randall, and A. Zahrai, 1997: Design and deployment of a portable, pencil-beam, pulsed, 3-cm Doppler radar. *J. Atmos. Oceanic Technol.*, **14**, 1502-1512.

Table 1. Rainfall accumulations (mm) measured by gauges across the Goodwin Creek catchment using manufacturer (*Mcal*) or individual gauge calibrations (*ICal*), and estimated by the KNQA radar at the gauge locations (*Radar*). Collected values are shown as well (*Collect*).

No	*Type*	*MCal*	*ICal*	*Collect*	*Radar*
1	ARS	22.6	23.4	23.4	27.0
1	COL			24.2	27.0
2	ARS	23.6	23.1		24.1
4	ARS	25.4	26.8		24.5
5	ARS	0.8	0.8		30.8
6	ARS	3.0	3.2		31.3
7	ARS	24.9	27.4		26.2
8	ARS	30.7	34.2		27.9
11	ARS	25.1	27.9		30.2
12	ARS	24.4	22.2		30.2
13	ARS	26.7	28.4		24.1
14	ARS	26.2	26.6		24.3
34	BEL	-	30.5	30.7	31.8
35	BEL	-	29.2	31.0	27.9
41	TXI	23.4	25.6	24.1	24.1
41	COL			26.2	24.1
42	TXI	25.4	27.3		31.7
43	TXI	26.9	28.4	21.6	34.1
43	COL			29.6	34.1
45	TXI	26.7	29.3		24.8
46	TXI	26.2	28.2	27.3	28.0
46	COL			27.1	28.0
50	sARS	26.2	25.0	25.1	24.5
50	bARS	26.9	30.0	30.5	24.5
50	TB3	25.2	24.2	26.1	24.5
50	COL1			26.6	24.5
50	COL2			27.1	24.5
50	DIS1	28.4	-		24.5
50	DIS2	-	-		24.5
50	BEL	-	23.9	26.7	24.5
51	BEL	-	25.1	25.1	20.3
51	COL			25.5	20.3
52	TXI	24.4	26.4		21.1
53	BEL	-	25.1	25.1	21.1
54	BEL	-	25.1	26.9	30.8
55	TXI	24.4	26.3		33.1
57	BEL	-	22.6	26.9	31.9
57	COL			27.1	31.9
61	BEL	-	21.6	23.1	22.6
62	TXI	2.5	2.7		22.4
63	TXI	23.9	25.5		22.2
64	BEL	-	24.9	25.9	22.9
64	COL			26.8	22.9
65	TXI	25.1	27.3	25.7	28.6
66	BEL	-	26.7	26.7	28.0